ISSN 2347-3487

# Complex Impedance Measurements on the Steady State Behaviors of a 10-cell PEFC Stack

Seiji Yoneda[1], Yoshihiro Ohno[2]
[1]Department of Electrical, Electronics and Information Engineering, Faculty of Engineering, Kanagawa University, 3-27-1 Rokkakubashi, Kanagawa-ku, Yokohama, 221-8686 Japan
yoneds01@kanagawa-u.ac.jp
[2]Department of Electrical, Electronics and Information Engineering, Faculty of Engineering, Kanagawa University, 3-27-1 Rokkakubashi, Kanagawa-ku, Yokohama, 221-8686 Japan
oonoy001@kanagawa-u.ac.jp

## ABSTRACT

Experimental studies on the behavior of a Polymer Electrolyte Fuel Cell (PEFC) stack were conducted by performing complex impedance measurements. Initially, the steady state characteristics of a 10-cell stack were measured, and the power function of the DC current was obtained to represent these characteristics. The frequency properties of the complex impedance apparatus were investigated in order to clarify the limitations of frequency measurement. The components of complex impedance, the real and imaginary parts, were rearranged into two vectors to analyze their frequency responses to power and output DC current.

## Indexing terms/Keywords

PEFC, steady state characteristics, complex impedance, fundamental frequency of Fourier expansion

ISSN 2347-3487

# 1.INTRODUCTION

As reported in numerous studies on the characteristics of fuel cells [1], complex impedance measurement using an impedance analyzer has become increasingly popular in analyzing the dynamic features of fuel cells in operation. The development of a fuel cell monitoring technique based on the measurement of dynamic impedance response during operation has recently been attracting much attention [2]. Although complex impedance was originally conceived as a database entry [3], the significance of its individual values in an engineering context has become a focus of interest. The authors used a circuit including a high-frequency oscillator and a high-pass filter to measure the impedance of a fuel cell in operation [4], followed by further measurements of complex impedance using an impedance analyzer [5]. As has been pointed out, complex impedance fails to retain some important data characterizing the fuel cell, because the quantity, based on the Fourier transform, is obtained via integration and averaging, and thus has little significance beyond a database entry. Interpreting the complex impedance in a way that helps analysis of the characteristics and operational stability of fuel cells is in fact useful. The present work discusses relationships of the complex impedance with the power generation characteristics of fuel cells based on measurements of operational parameters of a 10-cell PEFC stack under steady-state operation.

# 2. BRIEF DESCRIPTION OF APPARATUS AND METHOD

## 2.1. APPARATUS

### 2.1.1. PEFC SPECIFICATIONS

The polymer electrolyte fuel cells (PEFCs), provided by Chemix, were used in a 10-cell series stack, in view of the low output of the individual cells. Principal specifications of the cell are shown in Table 1. The fuel and oxygen channels are in a cross-flow arrangement. The gas channels are replicated.

**Table 1. Specifications of single cell**

| | |
|---|---|
| Differential pressure between fuel and air electrodes | ≤ 0.03 MPa |
| Gas pressure | ≤ Atmosphere pressure + 0.05 M Pa |
| Cell voltage | ≥ 0.35 V |
| Load current | ≤ 40 A |
| Operation temp. | RT - 90°C, Recommended temp. 65 - 80°C |
| Gas equivalent per 1 A | $H_2$: 7 - 7.5 cc/min. $O_2$: 3.5 - 3.75 cc/min. |
| Electrode area | 80 $cm^2$ |

The circuit used in the experiment is schematically shown in Fig. 1. Hydrogen and oxygen are supplied to the PEFC via humidifiers 1 and 2, respectively, at controlled flow rates. Hydrogen and oxygen discharged by the PEFC are dehydrated in the cooling tanks before being released.

ISSN 2347-3487

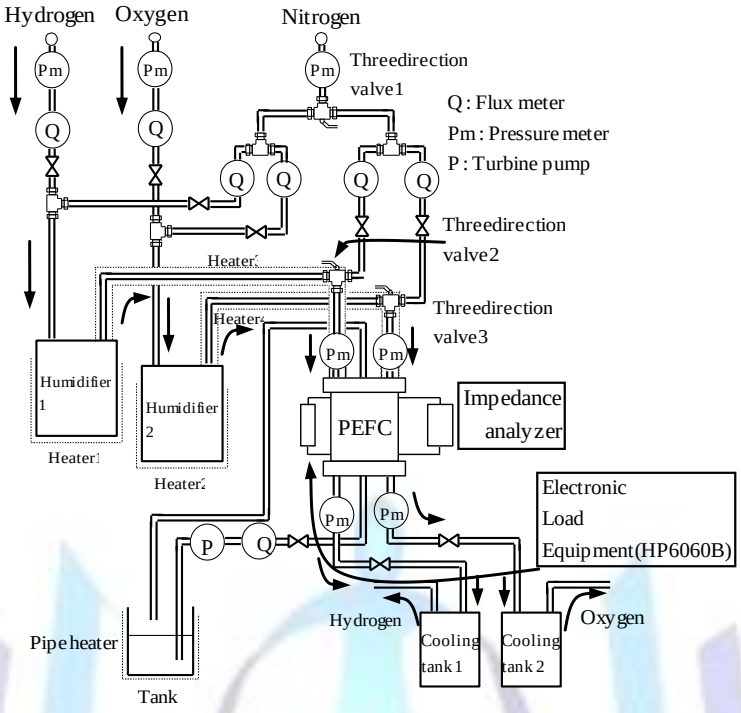


**Fig 1: Configuration of the experimental circuit**

## 2.1.2. VOLTAGE-CURRENT CHARACTERISTICS OF PEFC

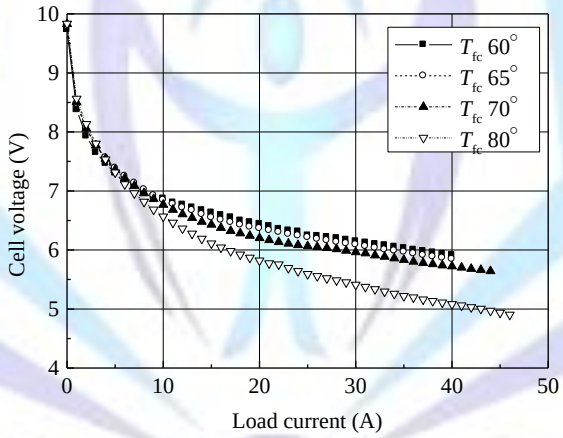


**Fig 2: Voltage-current characteristics of the 10-cell PEFC stack**

The voltage-current characteristics of the PEFC stack were measured at hydrogen and oxygen supply pressures of 0.1 MPa each and respective flow rates of 8.0 and 4.0 L/min., for different cell temperatures Tfc and humidifier temperatures. The results for a humidifier temperature of 60°C are shown in Fig. 2. For an operating point (*V*, *i*) in a steady state, fluctuation in output DC current by $i-\frac{d\,i}{2}$, $i+\frac{d\,i}{2}$ causes power fluctuation

$$\Delta W' = V\,d\,i \tag{1}$$

Similarly, voltage fluctuation by $V-\frac{dV}{2}$, $V+\frac{dV}{2}$ at the operating point causes power fluctuation

$$\Delta W'' = i\,d\,V \tag{2}$$

As far as a steady state is concerned, by choosing a constant $\alpha$ so that

$$\Delta W' - \alpha \Delta W'' = V\,di - \alpha\, i\, dV = 0$$

we obtain

$$V = a i^{1/\alpha} \tag{3}$$

where *a* and $\alpha$ are coefficients, the latter representing deviation from linearity. Thus, the static characteristics of the PEFC can be represented by a power function of current.

For example, the least squares fitting to the curve for $T_{fc}$ = 60°C in Fig. 2 gives

$$V = 8.617\, i^{-0.09858} \tag{4}$$

where $i \geq 1A$. Coefficients obtained in this way for each operating temperature are listed in Table 2. The coefficient $\alpha$ clearly increases with increasing operating temperature.

**Table 2. Coefficients of equation (3)**

| $T_{fc}$ (°C) | *a* | $\alpha$ |
|---|---|---|
| 80 | 9.312 | -6.2422 |
| 70 | 8.761 | -8.7489 |
| 65 | 8.688 | -9.5420 |
| 60 | 8.617 | -10.1440 |

When a sine wave current is superposed on the operating current as a disturbance, total current is

$$i = i_0 + \Delta i \sin(2\pi f t) \tag{5}$$

Therefore, using Eq. (3), the corresponding output voltage is,

$$\begin{aligned} V &= a\left(i_0 + \Delta i \sin(2\pi ft)\right)^{1/\alpha} \\ &= a\left(i_0^{1/\alpha} + \frac{1}{\alpha} i_0^{1/\alpha - 1} \Delta i \sin(2\pi f t) + \ldots\ldots\right) \\ &= V_0 + \frac{1}{\alpha}\frac{V_0}{i_0}\Delta i \sin(2\pi f t) + \ldots\ldots \end{aligned} \tag{6}$$

or, by neglecting the square and higher terms with respect to $\Delta i$ on the right side,

$$V - V_0 = \Delta V = \frac{1}{\alpha}\frac{V_0}{i_0}\Delta i \sin(2\pi ft) \tag{7}$$

Multiplying $\Delta V$ by $\sin(2\pi ft)$ and integrating and averaging over a period gives

$$\begin{aligned} \Delta \bar{V} &\equiv \frac{1}{\alpha}\frac{V_0}{i_0}\Delta i \frac{2}{T}\int_0^T \sin(2\pi ft)\sin(2\pi ft)\,dt \\ &= \frac{1}{\alpha}\frac{V_0}{i_0}\Delta i \end{aligned} \tag{8}$$

$$\Delta R \equiv \frac{\Delta \bar{V}}{\Delta i} = \frac{1}{\alpha}\frac{V_0}{i_0} = \frac{1}{\alpha} Z_{eq} \tag{9}$$

Therefore

$$Z_{eq} = \Delta R \alpha \tag{10}$$

Results are summarized in Table 3.

**Table 3. Comparison between calculations and measurements**

| $I$ (A) | 1 | 2 | 5 | 10 | 20 | 30 | 40 |
|---|---|---|---|---|---|---|---|
| $V_{cal}$ (V) | 8.617 | 8.047 | 7.35 | 6.867 | 6.41 | 6.16 | 5.99 |
| $V_{meas}$ (V) | 8.75 | 8.3 | 7.41 | 6.915 | 6.43 | 6.16 | 5.92 |
| $\Delta R_{cal}$ ($\Omega$) | 0.85 | 0.39 | 0.14 | 0.067 | 0.03 | 0.02 | 0.014 |
| $\Delta R_{meas}$ ($\Omega$) | 1.0 | 0.4 | 0.165 | 0.065 | 0.05 | 0.032 | 0.017 |
| $Z_{eq}$ ($\Omega$) | 8.617 | 4.02 | 1.47 | 0.686 | 0.32 | 0.20 | 0.15 |

The table shows $V_{cal}$, voltage calculated from the current by Eq. (4); $V_{meas}$, voltage read from Fig. 2; $\Delta R_{cal}$, resistance calculated by Eq. (9) from the parameters shown in Table 2; and $\Delta R_{meas}$, resistance obtained from the gradient of the curve shown in Fig. 2.

Complex impedance measurement starts with a sine wave of low frequency and proceeds to higher frequencies, because it is intended for measurement of the fundamental wave. The instrument always measures complex impedance for the fundamental wave, and the harmonics are eliminated by integration. In other words, the instrument provides signals regarded to be fundamental waves, and does not calculate any harmonic component in the response that is given by Eq. (3).

### 2.1.3. CAUTIONS TAKEN IN CONSTRUCTING THE EXPERIMENTAL CIRCUIT

The experiments were performed by supplying sine wave current from an impedance analyzer (Solartron SI 1260 or SI 1287) to the 10-cell PEFC stack, connected to a DC load equipment (HP 6060B), in steady state operation, and observing the response signals by an oscilloscope (Yokogawa DL 750). Results indicate that the current from the analyzer and the terminal voltage of the cell stack permit impedance measurement as far as the load current is kept strictly constant, since that the entire output current of the analyzer passes through the cell stack.

## 2.2. FREQUENCY CHARACTERISTICS OF THE IMPEDANCE ANALYZER OUTPUT

The frequency characteristics of the impedance analyzer were evaluated by replacing the cell stack with a DC power supply to confirm the current independence of the output frequency of the impedance analyzer. An AC current

$$i = \Delta i \sin(2\pi f t) \quad \Delta i = 0.76\ A_{peak} \tag{11}$$

was supplied from the analyzer to the DC power supply, and the waveforms of the output signal and the current at the load equipment (constant current control) were observed at different frequencies. The results are shown in Fig. 3, where the current waveforms at the DC power supply are shown on the left and those at the load on the right, for 100 Hz, 1 kHz, and 10 kHz from top to bottom. These plots show that the current at the load is maintained at 1.0 A; i.e., the AC current from the analyzer does not become part of the load. Separately, the frequency characteristics of the output impedance of the analyzer were also measured using a resistive load instead of the DC power supply. The result shown in Fig. 4 indicates that the output impedance of the analyzer decreases by about 3 dB around 455 Hz.

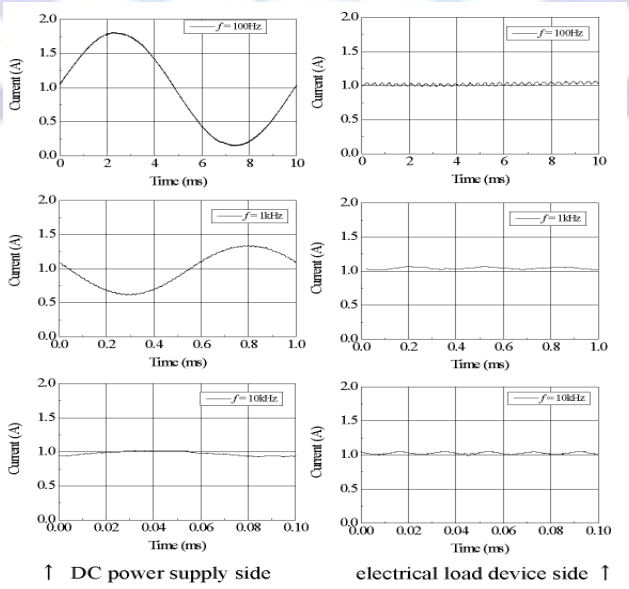


**Fig 3: Current waveforms from the DC power supply side and the electrical load device side**

ISSN 2347-3487

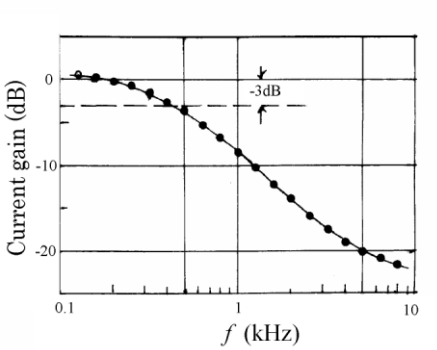


**Fig 4: Frequency performance of the output impedance from the impedance analyzer**

## 3. IMPEDANCE MEASUREMENT

Measurement of the complex impedance of a fuel cell indicates whether the internal processes in the cell can follow an AC current applied as a disturbance.

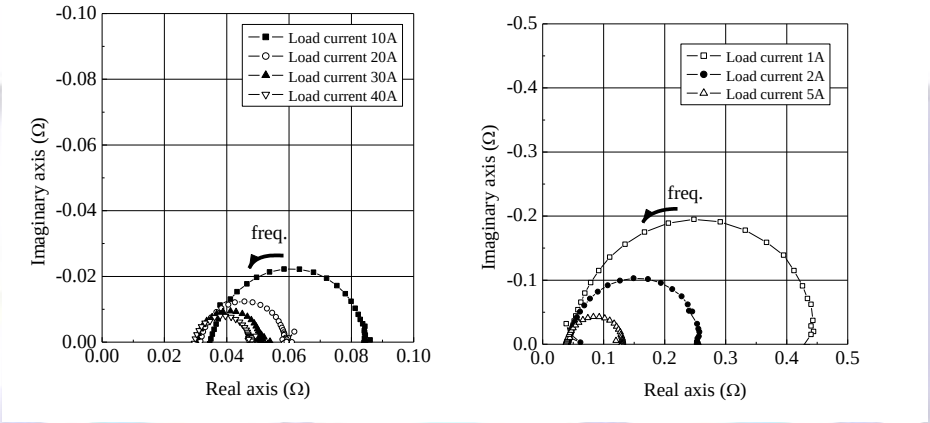


**Fig 5: Results of the complex impedance measurement**

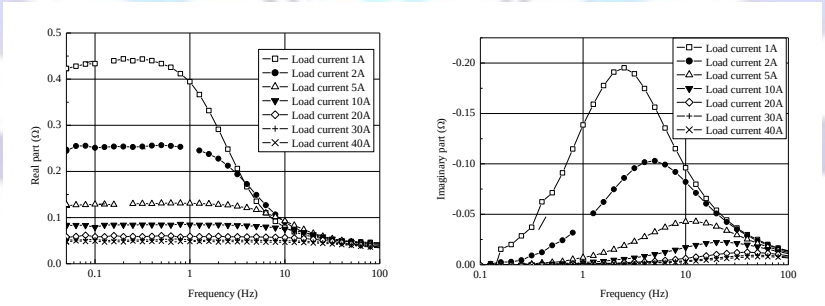


(a) (b)

**Fig 6: Frequency dependence of the real (a) and imaginary (b) parts**

Results: Fig. 5 shows, for different load currents, a typical impedance data plot for cell temperature 65°C, hydrogen and oxygen pressure 0.1 MPa each, humidifier temperature 60°C, hydrogen flow rate 8.0 L/min., and oxygen flow 4.0 L/min.

The abscissa represents the real part $z'$ and the ordinate the imaginary part $z''$. As shown earlier in measurements using a high-pass filter [4], the plot represents circles. The present results show size reduction of the circles with increasing output current.

The trajectory of the complex impedance is that of vectors

$$\left(z_1^{'}, z_1^{''}\right), \left(z_2^{'}, z_2^{''}\right), \ldots\ldots\ldots\ldots\ldots, \left(z_n^{'}, z_n^{''}\right) \quad (12)$$

These vectors are now rearranged to give two new vectors:

$$\left(z_1^{'}, z_2^{'}, \ldots\ldots\ldots\ldots\ldots\ldots, z_n^{'}\right) \text{ (real part vector)}$$

$$\left(z_1^{''}, z_2^{''}, \ldots\ldots\ldots\ldots\ldots\ldots, z_n^{''}\right) \text{ (imaginary part vector)} \quad (13)$$

Rearranging the vectors in Fig. 5 after Eq. (13) and plotting the real parts on the abscissa against the frequency of the fundamental wave on the ordinate (logarithmic) gives Fig. 6(a). Clearly, the real part is constant at very low frequencies: it depends solely on the load current and is independent of frequency. Meanwhile, it converges to a constant value independent of the frequency of the current applied or the load current. The convergence value of 0.04 Ω is considered to represent the internal resistance of the PEFC. Impedance change occurs between the two regions, or 1 Hz to 200 Hz. This means that the processes in the fuel cell are most susceptible to disturbances in the frequency range mentioned above. The behavior of the real part of the impedance shown in Fig. 6(a) is summarized as follows:

(I) For frequencies of applied AC current below a few hertz, the value is dependent on the bias current but not on the frequency of the external disturbance.

(II) It is frequency-independent for disturbances with fundamental frequencies above several tens of hertz.

(III) The real part of the complex impedance changes between these two regions, rapidly for small currents and more slowly for larger currents.

Similar calculations for the imaginary part of impedance resulted in Fig. 6(b).

Measurements with a constant DC output current of 10 A and amplitudes of the superimposed AC current of 50, 100, and 300 mA gave the same characteristics, so far as the amplitude is not excessively great. Since the internal characteristics of the fuel cell are more visible as functions of the DC current, it is convenient to use as the parameter the bias DC current rather than the amplitude of the superposed AC current.

Effects of temperature on complex impedance were not observed by measurements for different temperatures with an output current of 30 A.

The dependence of the complex impedance on the partial pressure of the gases was studied at cell temperature 65°C, hydrogen and oxygen gas pressure 0.1 MPa each, humidifier temperature 60°C, and output current 1 A and 30 A for different oxygen and hydrogen flow rates. The results shown in Fig. 7 indicate that the circle diameter may go through a minimum as the hydrogen or oxygen flow rate changes for small output currents, while remaining relatively stable for larger currents.

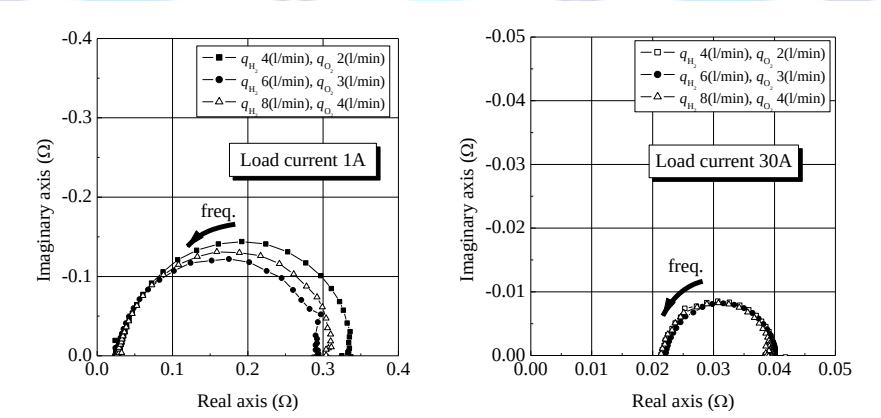


**Fig 7: Gas concentration dependence of complex impedance**

Multiplying the real part of the impedance shown in Fig. 6 by current gives power ( I = [J/C] = [J/As] = 1/A[W]), whose frequency dependence is shown in Fig. 8 (both axes are logarithmic).

When a fuel cell generates electricity, the concentration polarization increases temporarily due to formation of water. The polarization will, however, be decreased by further technical development. In an ideal situation, the circle would decrease in size as the current increases to approach a point where the value at high frequencies would coincide with that at low frequencies. With this in mind, the following analysis was conducted. For each curve in Fig. 8, two horizontal lines are drawn at the maximum value at the lowest frequency minus 10% the difference between the maximum and minimum values, and at the minimum value at the highest frequency plus 10% of the same. The intersections of the curve with

these lines are connected with a straight line, which gives a tangent to the curve. The intersections of the tangent with the two parallel lines are designated as flow and fhigh, respectively. In addition, the frequencies at which the absolute values of the imaginary part are maximum are determined, to obtain the relationship between frequency and load current as shown in Fig. 9. The gradient of the curve in the transient region is steeper and approaches 45° at smaller DC currents, whereas it decreases and approaches 0° at larger currents. In addition, the maximum current obtained from the PEFC was determined to be about 83 A.

The wavelength of the fundamental wave for which the impedance analyzer calculates the complex impedance (see 2.1.1 above) was determined as the intersection of the lines fimaginary and flow in Fig. 9 extrapolated to the low frequency and small current sides. This resulted in f = 2.0 mHz at 0.1 mA, indicating a very low fundamental frequency.

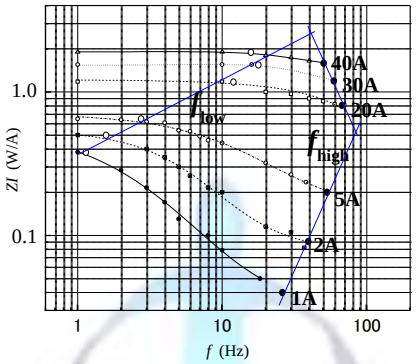


**Fig 8: Frequency dependence of power**

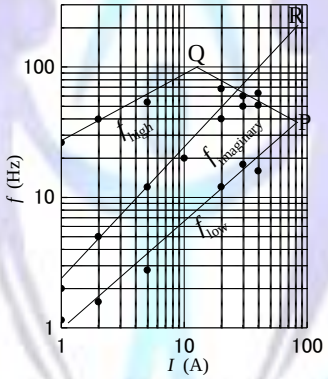


**Fig 9: Frequency dependence of electrical current**

## 4. DISCUSSION

Considering Eq. (8), a simultaneous linear equation can be established:

$$\begin{pmatrix} z_1^{'}, z_2^{'}, \ldots\ldots\ldots\ldots, z_n^{'} \\ z_1^{''}, z_2^{''}, \ldots\ldots\ldots\ldots, z_n^{''} \end{pmatrix} \begin{pmatrix} I_1 \\ I_2 \\ . \\ . \\ I_n \end{pmatrix} = \begin{pmatrix} e^{'} \\ e^{''} \end{pmatrix} \tag{14}$$

where $I_j$ is output DC current, and $e$' and $e$'' are applied voltages corresponding to the real and imaginary parts of impedance, respectively (not physically important). The relationship between the two current terms is discussed here. Since the rank of the [2, n] matrix on the left side of Eq. (14) is 2, any [2, 2] matrix equation can be derived from the matrix. Thus, two simultaneous linear equation systems are obtained:

$$z_1^{'} I_1 + z_2^{'} I_2 = e^{'}$$

$$z_1^{''} I_1 + z_2^{''} I_2 = e^{''} \tag{15}$$

Since the applied voltage has only the real component, the voltage corresponding to the imaginary part e" is zero. Then,

$$\left|\frac{I_1}{I_2}\right| = \left|\frac{z_2''}{z_1''}\right| \tag{16}$$

which means that the product of the imaginary part and the applied current, or the voltage W/A, is constant. For comparison with experimental results, the minima $z''_j$ in the curves in Fig. 6(b) were used. The results are summarized in Table 4.

**Table 4. Relationship between DC current and complex impedance**

| $I$ (A) | 1 | 2 | 5 | 10 | 20 | 30 | 40 |
|---|---|---|---|---|---|---|---|
| $f$ (Hz) | 2 | 5 | 12.5 | 20 | 40 | 50 | 63 |
| $Z''_j$ (Ω) | 0.196 | 0.104 | 0.044 | 0.022 | 0.012 | 0.008 | 0.0078 |
| $Z''_j I$ (V) | 0.196 | 0.208 | 0.22 | 0.22 | 0.24 | 0.24 | 0.312 |

These results confirm Eq. (16), although linearity is poor for large currents. Table 4 gives an average constant of 0.238. Furthermore, according to Table 4, the current is related to frequency as

$$f = 1.9508I \tag{17}$$

which is comparable with experimental data as shown in Table 5.

**Table 5. DC current vs frequency**

| $I$ (A) | 1 | 2 | 5 | 10 | 20 | 30 | 40 |
|---|---|---|---|---|---|---|---|
| $f_{cal}$ (Hz) | 1.95 | 3.90 | 9.75 | 19.5 | 39.01 | 58.5 | 78.03 |
| $f_{meas}$ (Hz) | 2 | 5 | 12 | 20 | 40 | 50 | 63 |

These results shown also in Fig. 9 reveal very good linearity. The intersection $R$ of the extrapolated line for the imaginary part and a vertical line passing through the intersection $P$ of $f_{high}$ and $f_{low}$ corresponds to 162 Hz and 83 A, whose ratio 1.9518 is in close agreement with Eq. (17). Although experimental data deviate from the equation at larger currents, the ratio 1.95 was confirmed for 83 A, which is the maximum current obtainable if no concentration polarization occurs. In other words, the frequency-current relationship for very small currents where effects of concentration polarization are negligible agree with what would be observed if no polarization occurred (i.e. the current of 83 A). The imaginary part of the complex impedance thus gives a linear relationship between frequency and DC output current at the apex of the circle.

## 5. CONCLUSIONS

The experimental results and discussion presented above can be summarized as follows.

(1) The resistance values calculated from the static characteristics of the fuel cell in steady-state operation approximate the measured values.

(2) Analysis of the imaginary part of the complex impedance shows that the DC output current is linearly related to the frequency of the superimposed current.

(3) The complex impedance can be analyzed with the frequency of the superimposed AC current as a parameter by rearranging the trajectory vectors ($z'_i$, $z''_i$) to form new vectors.

(4) The maximum current 83 A corresponding to zero concentration polarization and zero reaction resistance was determined by extrapolating the experimental data.

## REFERENCES

[1] For example, Nenryo Denchi, a quarterly journal published by FCDIC.

[2] J. Ross Macdonald: Impedance Spectroscopy, John Wiley & Sons, New York (1987).

[3] C. Andrews, P. Agarwal, T. Robinson and F. Büchi: “Integration maximizes returns on investment”, The fuel cell review, pp.23-28 (2005).

[4] K. Amanuma, Y. Kikuchi, Y. Ohno and J. Aoki: “ Measurement on Surface Impedance of SOFC during Operation”, 2000 ANNUAL MEETING RECORD I.E.E. JAPAN, pp.3369-3370 (2000-3).

[5] Y. Kikuchi, Y. Seki, S. Tannaka, T. Masuda, S. Yoneda and Y. Ohno: “Experimental Analysis of Impedance Characteristics of Electrode | Electrolyte Interface of a Polymer Electrolyte Fuel Cell”, 2005 ANNUAL MEETING RECORD I.E.E. JAPAN, pp.81-82 (2005-3).